

Research Article

Manufacturing of Filament for 4D Printing through Polyether-Type TPU/PLA Blend

Eun Joo Shin ¹, Ye Jin Song,¹ Yang Sook Jung,² Imjoo Jung,³ and Sunhee Lee ³

¹Department of Chemical Engineering, Dong-A University, 550-37 Nakdong-daero, Saha-gu, Busan, Republic of Korea

²Department of Biofibers and Biomaterials Science, Kyungpook National University, Daegu 41566, Republic of Korea

³Department of Fashion Design, Dong-A University, 550-37 Nakdong-daero, Saha-gu, Busan, Republic of Korea

Correspondence should be addressed to Eun Joo Shin; sejo06313@dau.ac.kr and Sunhee Lee; shlee014@dau.ac.kr

Received 26 September 2022; Revised 31 August 2023; Accepted 9 October 2023; Published 10 November 2023

Academic Editor: Surendar R. Venna

Copyright © 2023 Eun Joo Shin et al. This is an open access article distributed under the Creative Commons Attribution License, which permits unrestricted use, distribution, and reproduction in any medium, provided the original work is properly cited.

Reversible deformation structure fabricated by 4D printing can be applied in various fields, such as actuators, intelligent mechanisms, and soft robots. In this study, 4D filaments for use in fused deposition modeling (FDM) 3D printers were fabricated by melt extrusion process mixing polylactic acid (PLA) and soft actuator grade thermoplastic polyurethane (TPU) 75 Shore A. The morphological (scanning electron microscopy, atomic force microscopy), chemical (Fourier transform infrared), thermal (differential scanning calorimetry, dynamic mechanical analysis, thermogravimetric analysis), mechanical (Instron), and WAXS properties of the prepared TPU/PLA blend (5 : 5, 7 : 3, 9 : 1) filaments were investigated. Filaments of 4D auxetic reentrant TPU/PLA samples were 3D printed, and their shape-memory characteristics were assessed at temperatures of 60°C (corresponding to the glass transition temperature of PLA), 70°C, 80°C (matching the melting temperature of the soft segment of TPU), and 90°C. The properties of TPU/PLA samples differ based on the PLA to TPU ratio, with an increase in TPU content resulting in a higher shape setting temperature but a shorter shape recovery time. For the TPU/PLA 5 : 5 sample, setting at 70°C and recovering at 85°C is the most suitable condition for shape recovery, whereas for the TPU/PLA 7 : 3 sample the best conditions are setting at 80°C and recovering at 95°C. In the case of TPU/PLA 9 : 1, shape setting is possible at 90°C, and shape recovery is fastest at 95°C. A 4D structure of TPU/PLA could be achieved based on shape memory testing by temperature stimulation of 3D printed auxetic c TPU/PLA samples.

1. Introduction

Nowadays, “smart” materials or stimulus-responsive shape memory polymers have received great attention owing to their versatile employments to numerous fields, such as high-performance textiles, biomedical devices, actuators, packing films, heat-shrinkable tubes, and many others. 3D printing with smart materials produces 4D structures, for 3D printing methods, which include inkjet printing [1] stereolithography (SLA) [2] digital light processing [3], direct ink writing [4], and fused deposition modeling (FDM) [5, 6] are used. The FDM is the most popular 3DP technique due to its simple operating principle and cost-effective manufacturing process in comparison to other methods. 4D printing combines 3D manufacturing technology with shape memory materials to alter the shape or characteristics of the printed structure when exposed to

external triggers [7]. Also, many materials could be 3D printed with FDM. Although FDM usually utilizes thermoplastic materials, a variety of 3D printable composites have also been developed among them composites with micro- and nanoparticles, and bio-based material called polylactic acid (PLA) [8, 9]. Nowadays, many researchers try to create more opportunities of FDM 3DP applications by making functional objects and new designs with various composite materials.

Thermoresponsive shape memory polymers (SMPs) are smart polymeric materials that, when exposed to a temperature change, can revert from a deformed state (temporary shape) to their original (permanent) shape [10]. The typical mechanism of thermoresponsive SMPs is as follows: (1) The SMP can be deformed at a glass transition temperature (T_g) of the switch units. (2) The load is held constant, and the temperature drops below T_g or T_m . (3) After that, the load is

released to fix the temporary shape. (4) The material can regain its initial form upon reheating the deformed SMP. This sequence of four steps, leading to shape restoration, constitutes a thermomechanical cycle. However, when applied in practice, it consumes both a lot of energy for heating, and time, e.g., the initial heating time and cooling time [11].

SMPs require cross-links at junction points, which arise from the microphase separation of the hard and soft segments (SSs) within thermoplastic polyurethane (TPU). The polymer's initial shape and transition segments are determined by a phase transition temperature [12]. As the TPU is structurally easy to design of their structural properties, it has been developed as the shape memory applications [13]. The T_g and T_m of both, the hard segment (HS), which can be considered as the physical crosslinking, and the SS, which controls elasticity, can be controlled by the segmental composition of TPU. The SSs of TPU elastomers predominantly consist of either polyester or polyether. Some types of them have been reported to be miscible with PLA [14]. Poly(lactic acid) (PLA) can interact harmoniously with the soft polyether segments of TPU, establishing hydrogen bonds with the carbamates found in the HSs of TPU. Moreover, PLA exhibits shape memory behavior and is biodegradable, but its brittleness is a limiting disadvantage. PLA is among the commercially available biobased plastic materials known for its commendable properties and biodegradability. Nonetheless, its inherent brittleness restricts its applicability in various scenarios. Enhancing PLA's toughness through elastomer blending stands as an effective solution to this issue. Conversely, elastomers can be strengthened by incorporating them with rigid thermoplastics. Many possibilities of mixing mentioned materials create an opportunity to conduct vast amount of research [15–20] on the blendings of TPU and PLA. PLA and TPU are both biocompatible polymers employed in biomedical applications, and they have received approval from the FDA [13]. Since TPU is a suitable material to increase PLA toughness, the blending gives the TPU/PLA ideal strength, elasticity, and toughness. Hong et al. [15] demonstrated that the gradual incorporation of TPU elastomer into PLA can shift its fracture behavior from brittle to ductile. They achieved a more than threefold increase in notched impact strength by introducing 10 wt.% TPU. Lai et al. [16] showed that PLA/TPU (50/50) melt-blends have shape recovery ratio up to $(93.5 \pm 0.4)\%$ at 160°C . Leng et al. [17] reported that utilizing FDM technology, they effectively manufactured TPU-based soft components reinforced with in situ PLA microfibers. The outcomes can be ascribed to the effects induced during deposition, and they put forth a proposed mechanism for the formation of PLA microfibers. Boyacıoğlu et al. [18] focused on understanding the shape memory behavior of polyethylene glycol (PEG) plasticized PLA/TPU blends and suggested that plasticized PLA/TPU blends, incorporating lower molecular weight PEG (1,000 g/mole) and possessing the ideal PLA/TPU ratio, exhibit great potential for in vivo applications near human body temperature. Tao et al. [19] printed personalized orthosis with TPU/PLA composite filament by FDM, and revealed that the TPU/PLA composite filament is better suited for orthosis design compared to pure PLA. Jing et al. [20] conducted a study in which they formulated blends of PLA/TPU and observed intriguing shape memory

properties. Furthermore, they elucidated the shape memory mechanism of this PLA/TPU blend. In this mechanism, the crystalline regions of PLA function as anchoring points that help the material maintain its shape, while TPU serves as a stress concentrator that reinforces the rigid PLA, preventing it from fracturing during substantial deformation [20]. Upon heating, PLA molecules undergo a process of returning to their initial positions, thereby releasing stored energy. This energy release facilitates the restoration of the sample to its original shape. On the basis of previous TPU/PLA blend morphology and physical research results, the aim of this study is to prepare filaments with TPU/PLA blend pellets and manufacture 4D structure by FDM printer. Recently, we studied extrusion and filament manufacturing conditions and fabricated FDM 3D printable filaments with commercial and synthetic TPU pellets, which were used to create pliable actuators with a desired Shore A hardness ranging from 65 to 85 [21, 22].

This study focused on the manufacturing 4D structure with TPU/PLA blend stimulated by temperature. First of all, conditions must be established for the extrusion of TPU/PLA pellets and the subsequent filament fabrication process and shape memory properties with temperature stimuli. Through previous researches [21, 22], it was feasible to produce continuous filaments with constant diameter and hardness for 3D printers, making them suitable for use in the production of soft actuators. The shape memory property could be realized by compounding with PLA, and the ratio of PLA was set to less than 50% by weight to the ratio of TPU/PLA, and the shape memory property was designed to appear between 60 and 90°C , and their Shore A hardness was less than 95. Next, the chemical and physical properties were assessed in accordance with varying ratios of TPU/PLA. Subsequently, utilizing the characteristics of the filaments obtained, 4D auxetic reentrant TPU/PLA samples were 3D printed, and the shape memory properties of these samples were investigated.

2. Experimental




2.1. Preparation of TPU/PLA Blending and Filaments

2.1.1. Materials. Commercial TPU pellets of 75 Shore A (Dongsung Chemical, Korea) and PLA pellet (4032D, Nature work, USA) were used.

2.1.2. Blending. The PLA and TPU 75 Shore A pellets were dried at 50°C for 24 hr in vacuum dryer in order to eliminate moisture. The dried pellets were blended in weight ratios of 5:5, 7:3, and 9:1, and then extruded using a single-screw extruder (Filibot H400, Fordentech, Korea). Subsequently, the extrudates were cooled and pelletized. This extrusion and pelletization process was iterated 3–4 times to achieve thoroughly mixed TPU/PLA blend filaments.

2.1.3. Filaments. A TPU/PLA filament was prepared using a single-screw extruder (Filibot H400, Fordentech, Korea), and the nozzle diameter was set between 1.5 and 1.7 mm. A TPU/PLA filament with stable diameter and dimension could be manufactured with combination of various parameters. Table 1 displays the outcomes of the extrusion conditions, providing an overview of the melt-extrusion parameters

TABLE 1: Melt-extrusion parameters for TPU/PLA blend filament production from pellets.

Ratio of TPU/PLA items	5 : 5	7 : 3	9 : 1
First temperature (°C)	193	191	190
Second temperature (°C)	192	191	189
Third temperature (°C)	192	190	189
Screw speed (rpm)	12.0	12.0	13.2
Nozzle (mm)	1.5	1.5	1.5
Filament diameter (mm)	1.80 ± 0.10	1.80 ± 0.05	1.85 ± 0.05
Filament hardness (Shore A)	94	92	86
Products			

employed for the production of TPU/PLA filaments from the pellets. The pellet hardness is closely related to the operating conditions, the extrusion temperature in particular. When the content of PLA increase, filament extrusion is possible at a high screw temperature owing to the higher melting energy ($\Delta H T_m$ (J/g)) of PLA than TPU, which is associated with the differential scanning calorimetry (DSC) result. The TPU/PLA pellets with 5 : 5, 7 : 3, and 9 : 1 ratio could be extruded in the third process at 192, 190, and 189°C, respectively. During the fabrication process, filaments with a diameter of 1.80 ± 0.10 mm were obtained with a screw speed of 12.0–13.2 rpm.

2.2. 3D FDM Printing of Filament for 4D TPU/PLA. Following the extrusion of TPU/PLA filaments with varying TPU/PLA ratios, the output data in Cubicreator program (Cubicon Inc., Korea) were utilized to create auxetic reentrant (RE) structures. Before the 3D printing process, an initial test at 190–230°C was carried out to confirm the correct printing temperature and loading conditions. The 3D reentrant (RE) pattern was generated using the 123D design program by Autodesk Co., Ltd. (Korea), resulting in a sample measuring 30 mm × 30 mm with a thickness of 2 mm and a repeat size of 10 mm × 10 mm. During this process, the nozzle temperature for 3D printing was established through preliminary tests with TPU/PLA filament. The printing speed and infill rate were configured at 60 mm/s and 20%, respectively. The chosen design was then converted into a G-code file and printed using an FDM 3D printer (Cubicon Single Plus, TPC Mechatronics Corp., Korea).

2.3. Analysis of TPU/PLA Blend Filaments

2.3.1. Optical Microscopy. The TPU/PLA blended filaments were examined using an optical microscope (NTZ-6000, NEXTVISION, USA).

2.3.2. Scanning Electron Microscopy (SEM). The morphological characteristics of TPU/PLA blended filaments were analyzed using a scanning electron microscope (SEM) instrument, specifically the JSM-6400F model from JEOL, Japan, operated at 5 kV.

2.3.3. Atomic Force Microscopy (AFM). The surface morphology of TPU/PLA blended filaments was explored using the Inova system manufactured by Bruker. The system was equipped with a standard silicon nitride probe, specifically the Super Sharp Silicon™—SPM-Sensor from NanoSensors™, Switzerland, featuring a spring constant of 42 N and a resonant frequency of 320 kHz. These measurements were conducted under ambient conditions utilizing the tapping mode AFM technique. Surface images were taken in $20 \mu\text{m} \times 20 \mu\text{m}$ size. The bulk morphology was assessed by capturing images of the fracture surfaces after freeze fracturing the sheets at a temperature of -80°C . Subsequently, the AFM images were processed using NanoScope analysis software.

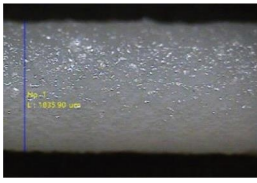
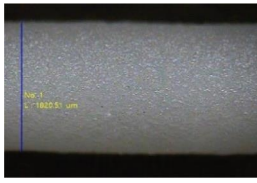
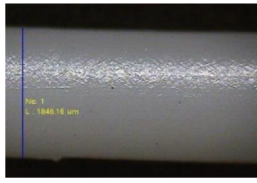
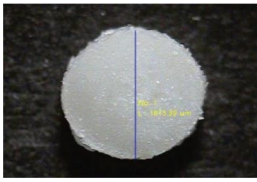
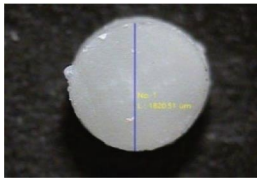
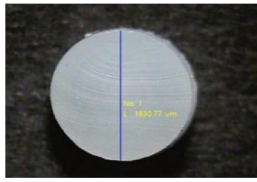
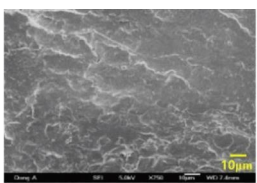
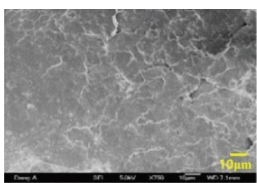
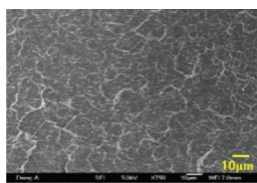
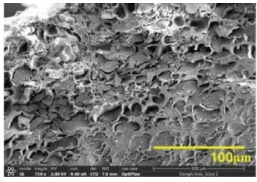
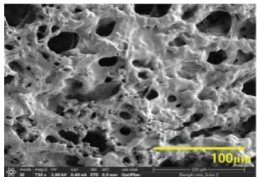
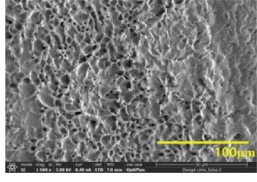
2.3.4. Shore a Hardness. Hardness was measured at room temperature (RT) using a Zwick Roell GS-706N from TECLOCK, Japan. This is analogical hardness testing apparatus, and following, “UNE-EN ISO 868:1998: plastics and ebonite”. Indentation hardness was determined by means of a durometer (Shore hardness) standard procedure at $(23 \pm 2)^\circ\text{C}$ and 50% relative humidity.

2.3.5. Fourier Transform Infrared (FTIR) Analyses. The molecular structures of the extruded TPU/PLA filaments were characterized using Fourier transform infrared (FTIR spectroscopy) with a Spectrum 100 instrument from PerkinElmer, USA, which was equipped with a diamond attenuated total reflectance accessory.

2.3.6. Differential Scanning Calorimetry (DSC) Analysis. The transition temperatures of the samples were determined using DSC with a DSC 8,500 thermal analyzer from TA Instruments, USA. Each sample weighed between 2 and 10 mg. The measurements were carried out over a temperature range spanning from -70 to 250°C , employing a heating rate of $20^\circ\text{C}/\text{min}$ under a nitrogen purge.

2.3.7. Thermogravimetric Analysis (TGA). The thermal stability of the extruded TPU/PLA filaments was assessed using a TGA Q500 instrument from TA Instruments, USA. The heating temperature range was configured from 30 to 600°C ,

TABLE 2: Microscope and SEM micrographs of TPU/PLA blend filaments.

Ratio of TPU/PLA item	5:5	7:3	9:1
Microscope	Surface section 		
	Cross-section 		
SEM (×750)	Cross-section 		
	Cross-section (partially removed TPU) 		

with a heating rate of 10°C/min, all conducted under a nitrogen atmosphere.

2.3.8. Dynamic Mechanical Analysis (DMA). The dynamic mechanical and thermal properties of the filament samples were evaluated using a DMA-Q850 instrument from TA Instruments, New Castle, USA. The measurements were conducted at a frequency of 1 Hz (with an amplitude of 2 µm and a preload force of 0.01 N) across a temperature range spanning from −100 to 150°C, employing a heating rate of 4°C/min. The samples had a cylindrical shape with a length of 13.09 ± 0.1 mm.

2.3.9. Tensilon Analysis. The mechanical properties of extruded filaments were measured for filaments with diameter 1.6 ± 3 mm using an Autograph tester (Instron 4201, Sidmazu, Japan) at RT and at speed of 100 mm/min.

2.3.10. WAXS Analysis. X-ray diffraction (XRD) analysis was performed using an XRD-6000 instrument from Shimadzu, Japan, operating at 40 kV and 30 mA with monochromatic CuKα radiation ($\lambda = 0.15418$ nm). Scans were conducted over the range of $2\theta = 5\text{--}60^\circ$ with a step size of 0.05° and a measurement time of 2 s per step (equivalent to a rate of 1.5° per min).

2.3.11. Shape Memory Test. To study the shape memory behavior of the 3D-printed TPU/PLA blends, the following steps were executed: (1) The original printed shape was

wrapped around a glass rod. (2) It was then placed in a 75°C oven for 5 min. (3) Subsequently, the sample was allowed to return to RT until thermal stress dissipated. (4) Finally, it was reheated at temperatures of 80, 85, and 90°C, sequentially, to recover its original shape.

3. Results and Discussion

3.1. Examination of the Morphology of TPU/PLA Blend Filaments. When polymer blend is made, the miscibility and morphology are pivotal to gain an understanding of its mechanical properties. Table 2 shows microscope and SEM imagery of the fractured filament.

3.1.1. Microscopic and SEM Analysis. The cross-sectional and side-sectional microscopic views reveal a cocontinuous and uniform surface, indicative of a well-mixed state and good miscibility. However, in the 5:5 TPU/PLA blend, nonuniformities appear on the filament surface, in comparison with the other samples. As the proportion of TPU increases, the surface and cross-section photos appear smooth due to for almost large amount of the TPU matrix, which PLA acts as a reinforcing agent. The observation is confirmed in the SEM micrograph of 9:1 TPU/PLA blend, which appears as very uniform white spots in the TPU matrix. In order to further analyze the morphology of each TPU/PLA blend, the samples were dissolved using a solvent, and then examined under the SEM. To dissolve the TPU phase on the surface of

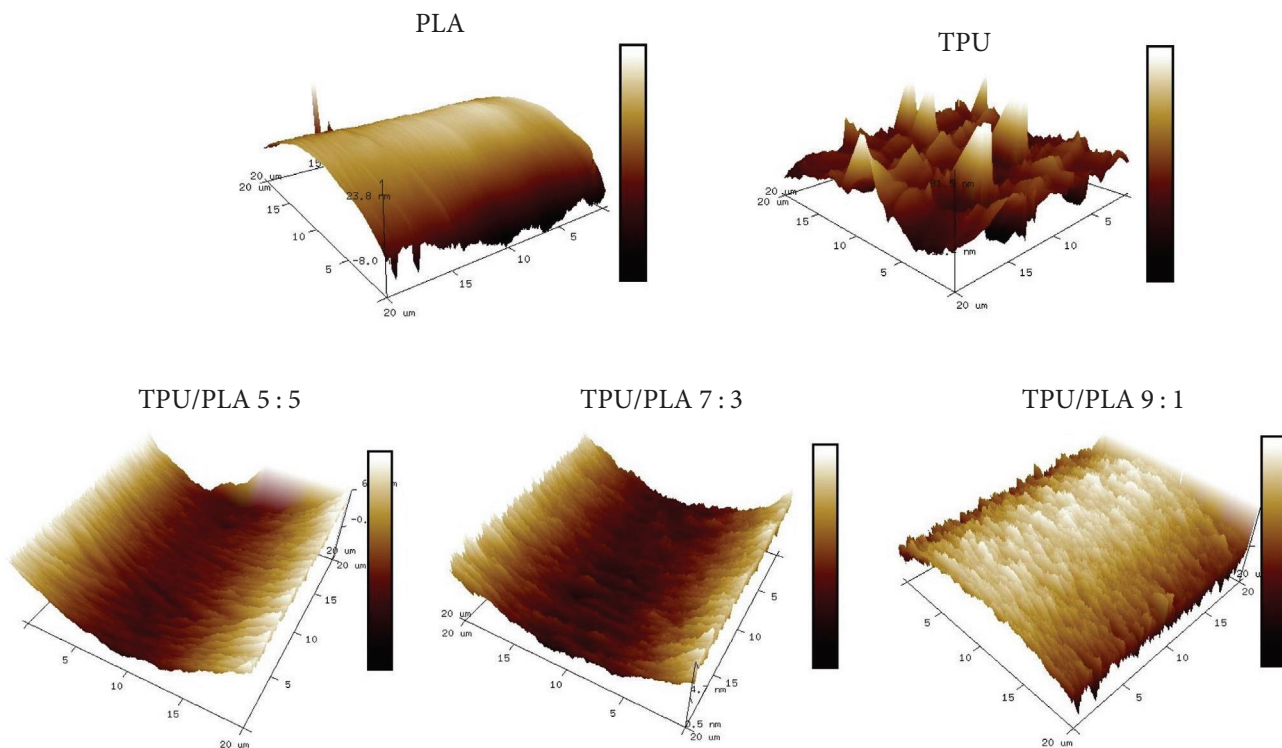


FIGURE 1: AFM images displaying the freeze–fractured surfaces of PLA, TPU, and TPU/PLA blend filaments.

filaments, dimethylformamide (DMF) was used. The SEM micrographs of the TPU/PLA 5:5 blend depicted a spongy PLA structure post TPU removal, indicating the persistent formation of this morphology. In samples with increasing ratio of TPU, particles of PLA reveal themselves as having globular structure.

3.1.2. Atomic Force Microscopy. Atomic force microscopy (AFM) was used to evaluate the miscibility of PLA and TPU domains in the TPU/PLA blends. While AFM is conventionally employed for observing surface physical structures and quantifying surface roughness [23–25], it also serves as a valuable tool for probing the internal structure of mechanically blended materials, particularly when making comparisons with other analytical methods is necessary. Figure 1 shows 3D AFM images of the PLA, TPU, and TPU/PLA blend samples using a tapping mode, while Table 3 presents the results. After freeze and fractured, cross-sections of the PLA sample are very regular and even, whereas TPU sample has an irregular and relatively rough surface. Furthermore, TPU exhibits two distinct types of phase contrast under examination: a dark and featureless matrix, which corresponds to the SS, and scattered bright elements of varying sizes dispersed within it. The dark matrix represents the SS, while the presence of numerous spherical globules indicates the phase-separated HS domains of TPU [26], respectively. The roughness in the Z-profile of TPU contributes to the cocontinuous network morphology [27] and shows an actual value of 17.6, as shown in Table 3. In the TPU/PLA blended samples, the roughness in the Z-profile (R_q) increases from 1.41 to 5.02 along with TPU proportion, which may have

TABLE 3: Characterization of the AFM results for the PLA, TPU, and TPU/PLA blend filaments.

Ratio of TPU/PLA items	PLA	5:5	7:3	9:1	TPU
Surface area (μm^2)	400	400	400	400	401
R_q (nm) ^a	10.7	1.41	4.55	5.02	17.6
R_a (nm) ^b	8.32	1.18	1.99	2.08	11.8
R_{max} (nm) ^c	10.1	7.82	11.28	11.41	10.36

Surface area: total area of examined sample surface. Mean: the average of all Z values within the enclosed area. ^a R_q (rms): the standard deviation of the Z values within the given area. ^b R_a (mean roughness): the mean value of the surface relative to the center place. ^c R_{max} (max height): the difference in height between the highest and lowest points on the surface relative to the mean plane.

significantly contributed to the roughness enhancement of the TPU. However, the overall surface roughness of the TPU/PLA blend samples are evenly formed, and the physical compatibility of the blends is satisfying because local domains of PLA or TPU do not appear.

3.2. Characteristics of TPU/PLA Filaments

3.2.1. Molecular Structure. Figure 2 illustrates the FTIR spectra of the TPU/PLA blend filament samples. The peaks observed at approximately $3,230\text{ cm}^{-1}$ are associated with the NH stretching vibration [28]. Peaks at $1,529\text{ cm}^{-1}$ can be attributed to CN stretching vibrations, while those at $1,597\text{ cm}^{-1}$ are indicative of NH bending vibrations of the urethane group within the TPU. Additionally, the peaks at $2,930$ and $2,858\text{ cm}^{-1}$ correspond to the asymmetric and

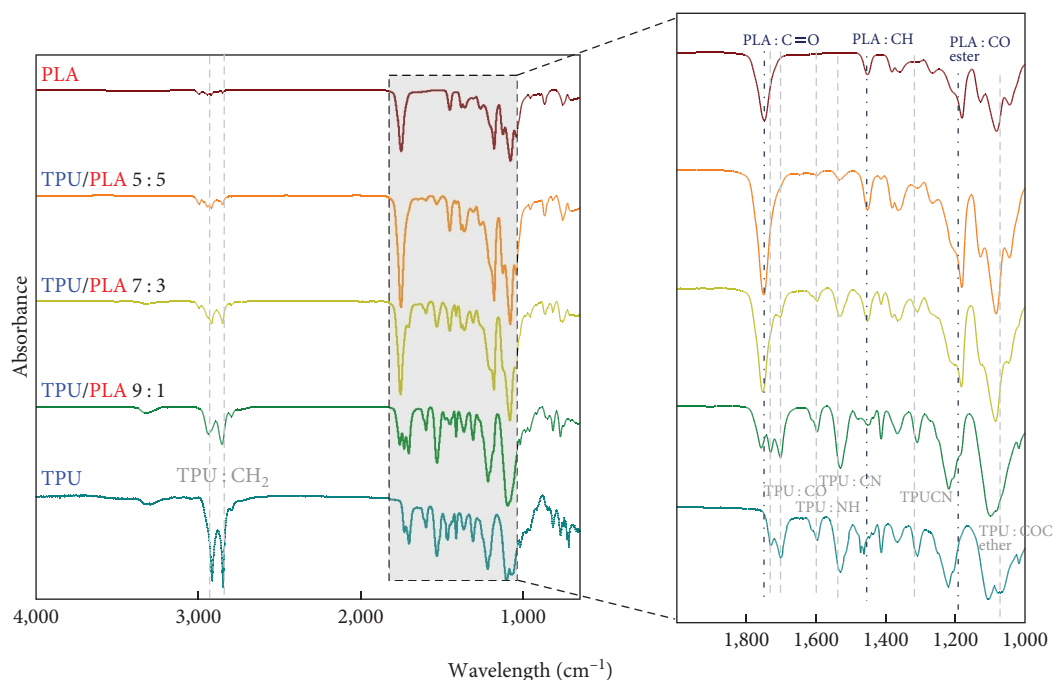


FIGURE 2: FTIR spectra of the PLA, TPU, and TPU/PLA blend filaments.

symmetric vibrations of CH_2 groups, respectively. Their intensity increases with increasing TPU proportion [29]. However, the intensity of $1,748\text{ cm}^{-1}$ (related to CO group) and $1,190\text{ cm}^{-1}$ (related to ester CO) peak in PLA decreases with increasing TPU proportion [30]. The double peak in range of $1,700\text{--}1,730\text{ cm}^{-1}$ is associated with $\text{C}=\text{O}$ stretching vibrations of which peak at $1,730\text{ cm}^{-1}$ is related to the free carbonyl group and at $1,700\text{ cm}^{-1}$ is related to the hydrogen-bonded carbonyl group [31]. In polyether type, like 75A TPU, there are two absorption bands, which appear at $1,700$ and $1,730\text{ cm}^{-1}$ [32–34]. The FTIR results suggest a successful blending of PLA and TPU without the emergence of any new chemical reactions. This shows that no chemical reaction occurred between TPU and PLA during melt mixing. Mi et al. [35] also found that PLA does not react with TPU.

3.2.2. Thermal Properties. (1) *Differential Scanning Calorimetry (DSC).* As shown in Figure 3 and Table 4, thermal transition temperature and the miscibility of the TPU/PLA blend samples are confirmed by DSC. Moreover, the most important factor for examining the temperature-stimulated shape memory performance is the heat transition temperature (T_{trans}). In order for a polymer to exhibit shape memory properties, it must possess two essential structural components: permanent net-points and reversible molecular switching segments [36]. The permanent net-points can be provided with chemical crosslinks, crystalline or other secondary phases, or macromolecular entanglements, resulting in a 3D network that prevents chain slippage/flow/creep upon deformation, allowing the storage or memory of permanent shapes, as well as interpenetrating networks. Conversely, the reversible molecular switching segments either stabilize the temporary shape or enable its transformation

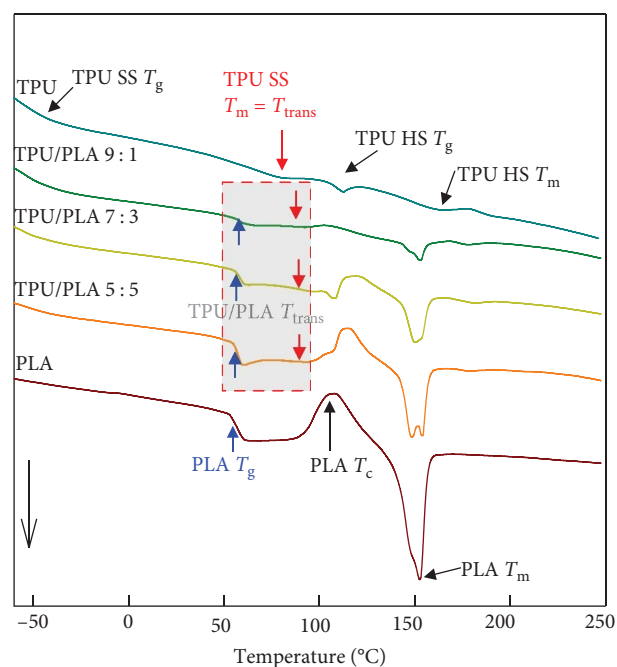


FIGURE 3: DSC results of PLA, TPU, and TPU/PLA blend filaments.

when triggered by a stimulus. This occurs through changes in molecular mobility that result from the formation or disruption of reversible interactions. This shape memory according to two elements can be accomplished during the glass transition temperature (T_g), or crystallization/melting transition (T_m), and it is termed T_{trans} . The T_{trans} of molecules that react reversibly on molecular switching segments with heat can be confirmed by DSC analysis. The T_g of PLA within the TPU/PLA blend corresponds to the T_{trans} temperature, at

TABLE 4: DSC results of the PLA, TPU, and TPU/PLA blend filaments.

Ratio of TPU/PLA items	TPU	9 : 1	7 : 3	5 : 5	PLA
TPU SS T_g ($^{\circ}\text{C}$)	- 41.7	- 40.5	- 40.4	- 36.9	-
TPU SS T_m ($^{\circ}\text{C}$)	75.5	82.6	88.2	89.5	-
PLA T_g ($^{\circ}\text{C}$)	-	58.0	57.3	57.2	57.0
PLA T_c ($^{\circ}\text{C}$)	-	103.7	116.9	114.1	108.1
PLA $\Delta H T_c$ (J/g)	-	0.7	4.0	7.1	17.5
TPU T_m ($^{\circ}\text{C}$)	161.2	149.1	149.2	148.4	-
PLA T_m ($^{\circ}\text{C}$)	-	153.0	153.8	153.4	152.6
PLA $\Delta H T_m$ (J/g)	-	2.6	6.8	12.8	23.4

which the shape memory property is demonstrated. It is necessary to check the transition temperatures of the SS and HS for shape memory property of TPU. In TPU with elastic properties, when the shape is changed by an external force and returns to its original shape when the external force is removed, the HS becomes a permanent net-point and the SS becomes a reversible molecular switching segment. Therefore, the phase separation of HS and SS is important to provide the elastic properties of TPU. In general, the thermodynamic incompatibility between the SS and the HS in the elevated temperature process causes phase separation in a TPU material, resulting in peaks at the T_g , T_m of SS and the T_g and T_m of HS, respectively [37]. There are four broad peaks of TPU on the endothermic curves at around -40 , 80.3 , 105 , and 160°C , which correspond to SS T_g , SS T_m , HS T_g , and HS T_m , respectively.

For PLA sample, there are two endothermic peaks observed at 57 and 152°C , corresponding to T_g and T_m , respectively, as well as one exothermic peak at 108°C , representing T_c . The results from TPU/PLA blends do not indicate any significant shift in peak temperatures. However, there is an observable increase or decrease in peak intensity at the transition temperature as the blend ratio varies. Specifically, as the TPU content increases, the intensity of PLA-related peaks decreases, while the TPU-related peaks appear simultaneously. This observation leads to the conclusion that the two substances do not undergo chemical reactions with each other but exhibit excellent physical miscibility. For TPU/PLA, the PLA crystal peak continues to appear, so it can be concluded that PLA crystal is formed in the TPU matrix. The shape memory phenomenon caused by the temperature stimulation of the elastomer polymer appears near the melting temperature of the SS of polymer. Since the melting temperature of the SS is about 75°C and the intensity of the peak is rather weak, it is difficult to show the shape memory ability by temperature stimulation for TPU. As PLA contents increase, the melting temperature of the SS increases to 83 – 90°C although very subtle. Hence, it is reasonable to anticipate that the shape memory capability of TPU/PLA for achieving 4D properties will manifest at temperatures approximately ranging from 60 to 80°C due to the blending with PLA, which aligns with the T_{trans} for SMPs. Moreover, it was confirmed that the shape memory phenomenon appeared near this temperature in the

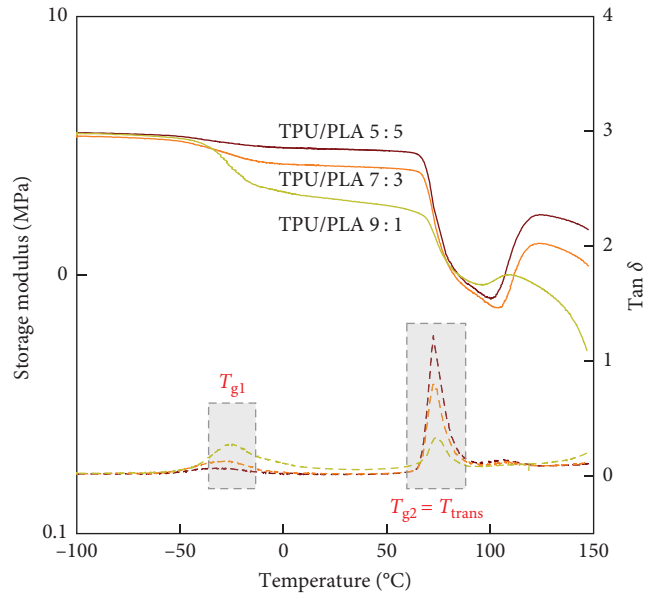


FIGURE 4: DMA graphs of the TUP/PLA blend filaments.

subsequent shape memory test. From this shape memory, the 4D structure of TPU/PLA could be accomplished.

(2) *Dynamic Mechanical Thermal Analysis (DMA)*. Figure 4 illustrates the storage modulus and $\tan \delta$ as functions of TPU/PLA samples with varying blend ratios. The storage modulus refers to the energy stored by an elastic material under deformation and provides information on polymer stiffness [38]. The high and consistent values of the storage modulus at low temperatures indicate the characteristic behavior of a glassy state. At -50°C , the drop in storage modulus is attributed to the glass transition of the SSS in TPU. This slope increases more rapidly, in accordance with the TPU content, and the decrease is greater. The second onset of storage modulus decrease occurs at 60°C related to the glass transition of PLA, which is progressively steeper with an increase in PLA proportion. The presence of increase above 100°C after the intense decrease in storage modulus indicates the recrystallization of PLA segments. T_g is the temperature at which the maximum of $\tan \delta$ for the polymer is reached. The $\tan \delta$ value reflects the ratio of energy loss and energy storage, signifying the glass transition of

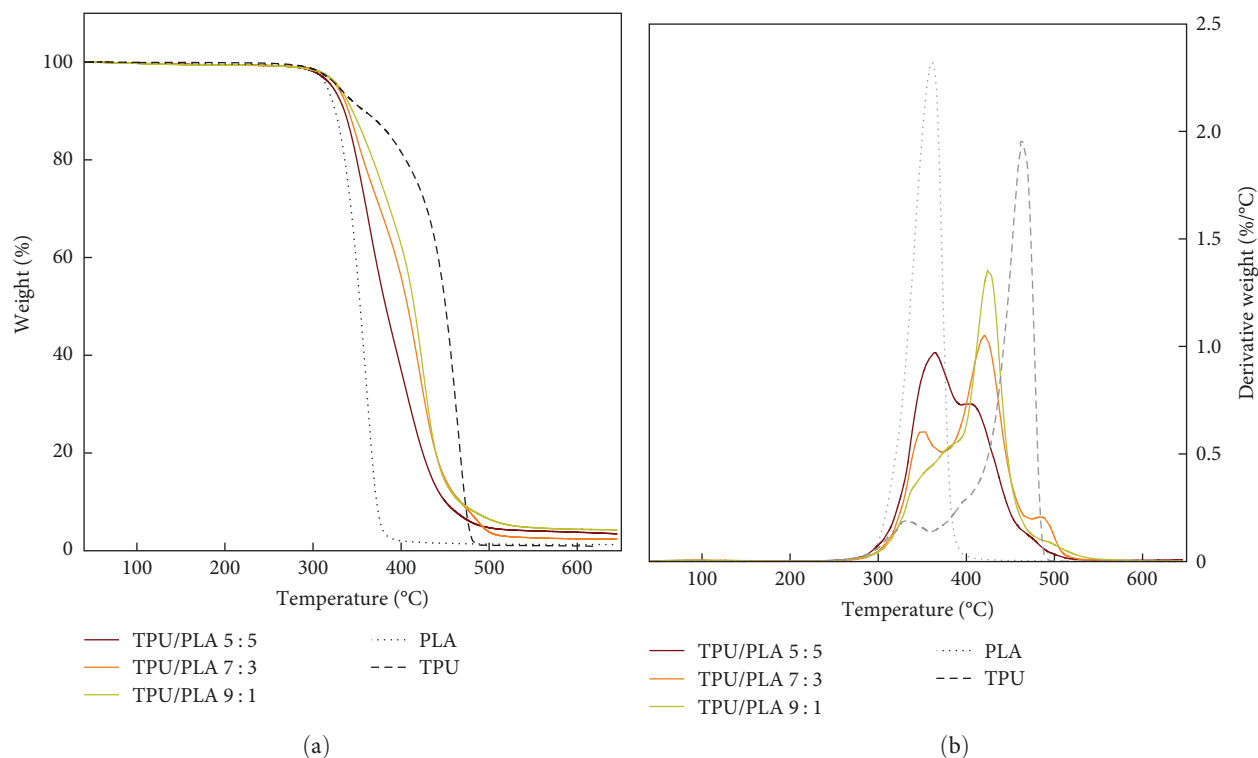


FIGURE 5: (a) TGA and (b) DTG curves of the PLA, TPU, and TPU/PLA blend filaments.

amorphous polymers within semicrystalline materials [34]. The $\tan \delta$ was observed at around 73°C and attributed to the PLA amorphous region, which intensity decreases with ratio of TPU. The maximal intensity of the second peak in $\tan \delta$ at around -27°C is related to the increases in the transition temperature of TPU SS. The DMA results for the TPU/PLA blend show the appearance of $\tan \delta$ corresponding to T_g peaks for each polymer respectively, instead of new peaks caused by the chemical interaction between TPU and PLA molecules. Additionally, only the difference in peak intensity caused by mechanical miscibility occurred. These results are similar in the DSC and FTIR analysis.

(3) *Thermogravimetric Analysis (TGA)*. Figure 5 displays the TGA curves and derivative thermograms (DTG) of the TPU/PLA blend samples. The thermal decomposition curve of TPU shows the first step at 330–370°C, associated with HS decomposition and the second step at around 450°C correlated with SS decomposition [39]. The thermal degradation of PLA occurs in a single weight loss step, as evident from the DTG curves. However, a delay of degradation is observed for the TPU/PLA blend from the onset temperature, which may be attributed to the increased proportion of TPU. Moreover, the single loss step curve changes to a two-step decomposition with the blend to TPU. In the case of TPU/PLA 5:5, degradation peaks are observed at 370 and 420°C. The former peak corresponds to the degradation of PLA and the SSs of TPU, while the latter is related to the degradation of the HSs of TPU. As the proportion of TPU increases, the peak intensity corresponding to the degradation of PLA and SS of TPU gradually decreases, and the peak intensity associated

with the degradation of HS of TPU, while the temperature range gradually increases toward higher temperature. This leads to the conclusion that as the TPU content increases, the thermal stability of the TPU/PLA blend becomes more robust and resistant to degradation.

3.2.3. X-Ray Diffraction (XRD) Properties. To determine an information of crystalline miscibility between TPU and PLA, the XRD measurement was performed, as shown in Figure 6. Figures 6(a) and 6(b) are XRD results measured for 3D printer filament having a diameter of 1.7 mm and a film pressed at 150°C, respectively. In Figure 6(a), the broad peak in the TPU sample at $2\theta = 19.5^\circ$ generally corresponds with the hydrogen-bonded hard domain between urethane groups [40]. The sharp peaks of 21.5° and 23° are associated with soft crystalline domains in soft and HSs, which are separated by the degree of microphase separation [41]. The peak of PLA shows a broad diffraction curve, which can be attributed to the fast cooling rate in the filament extrusion process. The XRD curve for the TPU/PLA blends also changed with one broad, almost amorphous peak at about $2\theta = 20^\circ$ for filament production under quenching condition through the extruder. In Figure 6(b), PLA sample, which was heat treated at 150°C for film formation, shows clear diffraction peaks at $2\theta = 15^\circ, 16.7^\circ, 19.1^\circ, 22.4^\circ,$ and 27.4° corresponding to the (010), (110/200), (203), (204), and (207) plans [42], respectively. The strength of crystallization peaks decreased as the TPU content increased. The distinct crystallization peak of PLA remains evident even when blended with TPU, suggesting that TPU and PLA are immiscible.

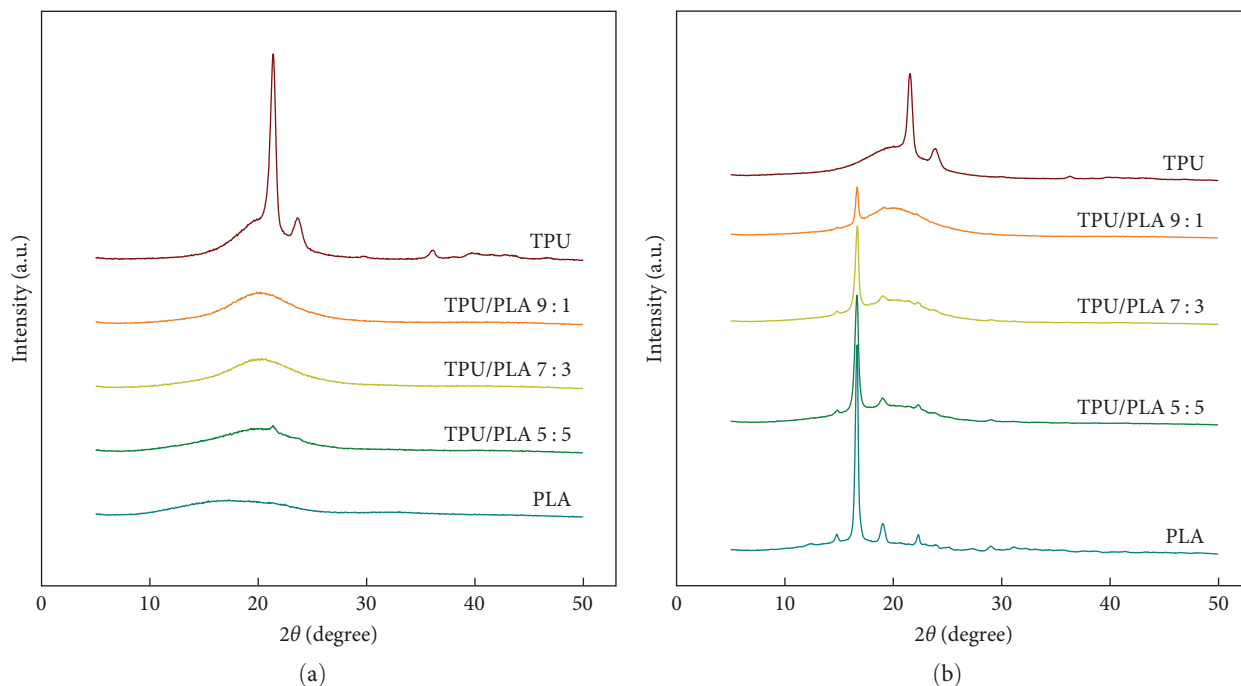


FIGURE 6: XRD patterns of the PLA, TPU, and TPU/PLA blends. (a) Filaments for 3D printer and (b) films pressed at 150°C.

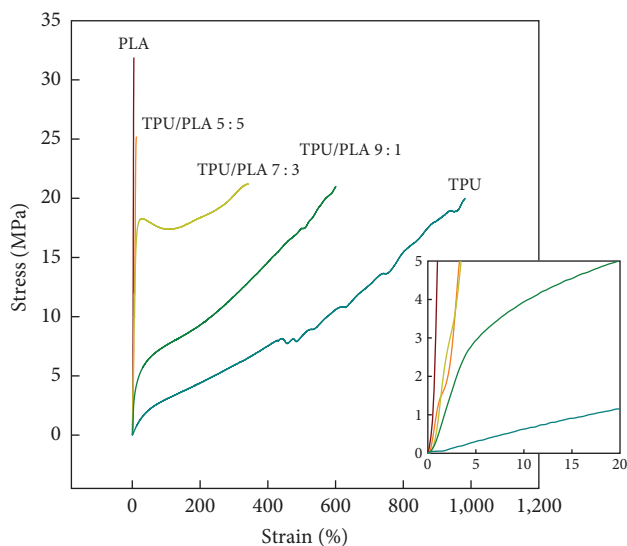


FIGURE 7: Stress–strain curves of the PLA, TPU, and TPU/PLA blend filaments.

3.2.4. Mechanical Properties. Figure 7 and Table 5 present the tensile stress–strain curves of the TPU/PLA blend filaments, which were fabricated using a melt extruder at RT. Figure 7 shows that the PLA sample has almost no plastic deformation and undergoes brittle fracture. The TPU/PLA blend samples demonstrate plastic deformation and ductile fracture behavior after passing the tensile yield point. A fore-mentioned properties of samples show that higher TPU content results in greater tensile toughness. Table 5 illustrates that the tensile modulus of the samples gradually decreases with an increase in the TPU ratio. While the tensile strength

of the TPU/PLA blends remains relatively unchanged, the elongation at break in the TPU/PLA 9:1 blend increases by over 700%. The tensile strength and elongation of the TPU/PLA 9:1 samples are measured at 24.25 MPa and 700%, respectively. The phase-separated HS and SS of TPU, which molecular chain exhibits unique properties of flexibility and elasticity, cause the increase of plastic deformation of the TPU/PLA blends. Owing to the contrast in elastic properties between the pliable TPU and the rigid PLA, stress concentrations initially emerge within the TPU domains when external forces are exerted on the samples. This results in elastic deformation within the TPU phase and the accumulation of deformation energy, accompanied by energy dissipation due to cavitation and partial separation. At the same time, the PLA matrix is plastically deformed. Described process might provide an explanation, why the PLA matrix exhibits good ductile behavior with increased TPU domains [20]. Moreover, the hydrogen bonds formed between PLA and TPU molecules ensure that with an optimal TPU content ratio, not only does the tensile strength of the blend samples not experience a substantial decline but also an increase in material deformation without fracture occurs.

3.3. 3D FDM Printing of Filaments for 4D Structure. Before performing 3D printing, a pretest was conducted at 190–230°C, as shown in Table 6, in order to confirm the suitable temperature and loading conditions for printing. For TPU/PLA 5:5, setting the loading temperature of the FDM to 190°C is not suitable, because it was injected with low viscosity. For the TPU/PLA 7:3 blend, it was observed that the extrusion process proceeded smoothly at 220°C, yielding a uniform surface. However, at 230°C, the melt viscosity reduced to a sticky

TABLE 5: Mechanical properties of the PLA, TPU, and TPU/PLA blend filaments.

Ratio of TPU/PLA items	0:10	5:5	7:3	9:1	10:0
Diameter (mm)	1.7 ± 0.03	1.7 ± 0.05	1.8 ± 0.05	1.6 ± 0.07	1.8 ± 0.05
Stress (MPa)	31.89 ± 0.7	25.21 ± 0.5	21.20 ± 0.4	20.99 ± 0.5	19.99 ± 0.3
Strain (%)	4.65 ± 0.1	12.49 ± 2.0	342.82 ± 4.7	600.98 ± 5.5	982.32 ± 7.3
Initial modulus (MPa)	1207.58 ± 0.05	296.55 ± 0.03	192.30 ± 0.05	40.86 ± 0.03	5.97 ± 0.05
Rupture energy (J)	0.04 ± 0.01	0.41 ± 0.01	3.92 ± 0.02	3.88 ± 0.03	5.33 ± 0.05

TABLE 6: Loading and product photos from pre test before 3D printing.

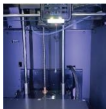





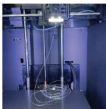

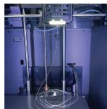





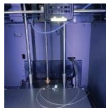















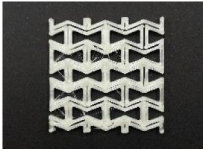
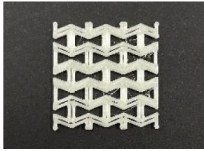
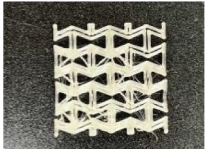
Temp. of loading ratio of TPU/PLA	190°C		200°C		210°C		220°C		230°C	
	Loading	Product	Loading	Product	Loading	Product	Loading	Product	Loading	Product
5:5										
7:3										
9:1										

TABLE 7: Images of auxetic reentrant (RE) TPU/PLA samples prepared using various TPU/PLA ratios are presented below.

Ratio of TPU/PLA items	5:5	7:3	9:1
Image			
Nozzle temp. (°C)	210	220	220
Weight (g)	1.09	1.01	0.89

The printing time for all 3D prints was 10 min and 45 s.

consistency, resulting in an uneven product surface with a wave-like pattern. In the case of TPU/PLA 9:1, the viscosity was excessively high, leading to frequent nozzle clogging at 190 and 200°C due to the elevated viscosity. However, at 220°C, the surface of the printed fiber appeared smooth.

Table 7 shows 3D-printed images of blend samples prepared from pellets of various ratios of TPU to PLA. The optimal extrusion temperatures for TPU filament in TPU/PLA 5:5, TPU/PLA 7:3, and TPU/PLA 9:1 were determined to be 210, 220, and 220, respectively. The extrusion test results revealed that TPU/PLA 5:5 exhibited good melting behavior even at lower extrusion temperatures, leading to a higher extrusion rate. The printed material was hard

and showed no elastic properties. However, it turns to soft elasticity with increase content of TPU. The 3D-printed sample of TPU/PLA 9:1 exhibited a smooth and glossy appearance. In terms of surface area, it was observed that the extruded lines in the printed object showed minimal protrusion along the nozzle's path of movement compared to other samples, resulting in neatly stacked layers.

3.4. Shape Recovery Properties of 4D TPU/PLA Structure. It is known that TPU readily undergoes deformation under a load applied at RT ($<T_m$ of the TPU SS), indicating that the recovery rate did not maintain the deformed shape. This strong elastic behavior is attributed to the presence of

TABLE 8: Shape memory testing of 3D-printed TPU/PLA blend samples under temperature stimulus.

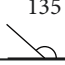
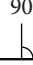
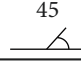
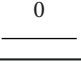

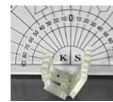
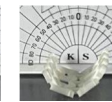
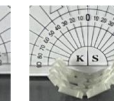

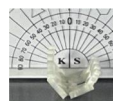
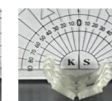
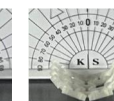



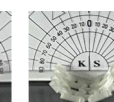

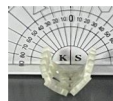
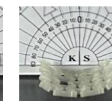
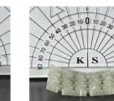

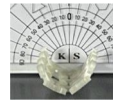
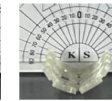
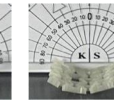

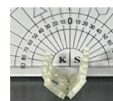

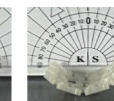
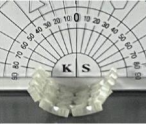
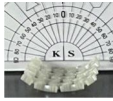

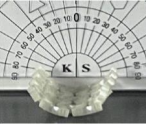


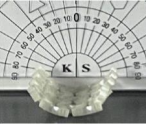
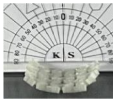








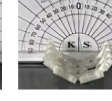
Samples	Recov. temp. (°C)	Angle (°) item	135	90	45	0
						
TPU/PLA 5 : 5 at 60°C (5 min)	65	Shape				
		Time (s)	15	50	90	230
	70	Shape				
		Time (s)	10	40	70	210
	75	Shape				
		Time (s)	15	40	60	200
TPU/PLA 7 : 3 at 60°C (5 min)	65	Shape				
		Time (s)		20	30	80
	70	Shape				
		Time (s)		15	30	60
	75	Shape				
		Time (s)		10	20	50
TPU/PLA 9 : 1 at 60°C (5 min)	65	Shape				
		Time (s)		10	30	
	70	Shape				
		Time (s)		8	20	
	75	Shape				
		Time (s)		5	10	
TPU/PLA 5 : 5 at 70°C (5 min)	75	Shape				
		Time (s)		25	40	75
	80	Shape				
		Time (s)		25	40	75

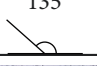
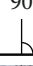
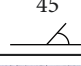
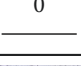






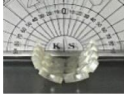
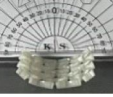

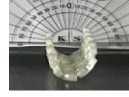
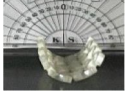

TABLE 8: Continued.

Samples	Recov. temp. (°C)	Angle (°) item	Angle (°)			
			135	90	45	0
TPU/PLA 7:3 at 70°C (5 min)	85	Shape				
		Time (s)	20	40	75	110
	75	Shape				
		Time (s)	30	50	65	110
	80	Shape				
		Time (s)	20	40	60	105
	85	Shape				
		Time (s)	20	40	60	95
TPU/PLA 9:1 at 70°C (5 min)	75	Shape				
		Time (s)		10	20	80
	80	Shape				
		Time (s)		5	15	60
	85	Shape				
		Time (s)		5	10	55
TPU/PLA 5:5 at 80°C (5 min)	85	Shape				
		Time (s)	40	55	90	150
	90	Shape				
		Time (s)	20	40	70	135
	95	Shape				
		Time (s)	20	40	65	110
TPU/PLA 7:3 At 80°C (5 min)	85	Shape				
		Time (s)	20	35	60	105

TABLE 8: Continued.

Samples	Recov. temp. (°C)	Angle (°) item	135	90	45	0	
	90	Shape					
		Time (s)	20	30	55	100	
	95	Shape					
		Time (s)	20	30	50	90	
	TPU/PLA 9 : 1 at 80°C (5 min)	85	Shape				
			Time (s)		10	30	65
		90	Shape				
			Time (s)		10	25	60
95		Shape					
		Time (s)		10	20	55	
TPU/PLA 5 : 5 at 90°C (5 min)		95	Shape				
			Time (s)	40	80	240	
		100	Shape				
			Time (s)	20	60	210	
		105	Shape				
			Time (s)	110	140		
TPU/PLA 7 : 3 At 90°C (5 min)	95	Shape					
		Time (s)	110	240	330		
	100	Shape					
		Time (s)	80	150	225		
	105	Shape					
		Time (s)	50	130	190		

TABLE 8: Continued.

Samples	Recov. temp. (°C)	Angle (°) item	135	90	45	0
						
TPU/PLA 9 : 1 at 90°C (5 min)	95	Shape				
		Time (s)	10	40	70	120
	100	Shape				
		Time (s)	10	40	80	145
	105	Shape				
		Time (s)	10	80	115	155

hard-segmented structures that act as physical cross-links within the material. When the external force is removed, certain internal stresses are released, resulting in a gradual rate of shape fixation. On the other hand, if the load is removed after applying an external force above the T_m of the SS, the shape is retained, and when the temperature is elevated beyond the T_m of the SS, it can be restored to its original state. However, in most conventional TPUs, the melting energy of the SS is insufficient to clearly exhibit shape memory. On the other hand, PLA is rigid and brittle at RT ($<T_g$ of PLA), and it easily deforms and retains its shape when the external force is removed if it is above the T_g . Nevertheless, even if the temperature surpasses the deformation temperature, it lacks shape memory capability. In the case of TPU/PLA blends, the T_{trans} temperature of blend samples is around 55–65°C due to the T_g of PLA based on the DSC result. Therefore, shape memory with temperature stimuli can occur with the above T_{trans} of TPU/PLA blend samples, as shown in Table 8 and Figure 8, which is our final purpose to manufacture of 4D TPU/PLA structure.

In order to explore the temperature-dependent shape-memory properties of the 4D printed reentrant (RE) structure, the setting and recovery temperature and the unfolding angle (135°, 90°, 45°, and 0°) over time were investigated. The shape recovery characteristics depending on the unfolding angle and time are shown in Table 8 and graphically illustrated in Figure 8. In Figure 8, the recovery ratio (%) was set to 100%, 75%, 50%, and 25% when fully unfolded at 0°, 45°, 90°, and 135°, respectively. Based on the DSC results obtained after 3D printing, deformation was induced in the temperature range of 60–90°C. It was observed that the 3D arch form could be readily restored to its initial flat shape (unfolding angle of 0°). The recovery process was documented using a digital camera, and the relationship between recovery ratio and recovery time (as shown in Figure 8) was analyzed using the images captured (as listed in Table 8). From the results in Figure 8 and Table 8, it can be seen that

the 3D-printed RE structure has shape memory properties, resulting in 4D RE structures. It was observed that when the 3D-printed RE structure was set at various temperatures, the arch-form quality improved as the temperature increased. At lower setting temperatures, it can be seen that the RE structure bends less with increasing TPU content. As the set temperature increases, the enhancement of the arch-form is attributed to the higher TPU content. Although the shape is restored after setting, the time required to transition from 90° to 45° in the arch-form follows a similar pattern, but there is a discrepancy in the time needed to achieve the final curvature (0°). The detailed results for each sample are as follows:

3.4.1. For TPU/PLA 5:5. Excellent setting is achieved at 60°C, and the shape recovery ratio reaches 100% at recovery temperatures of 65, 70, and 75°C, albeit with longer complete recovery times compared to other samples. When the temperature exceeds T_g of PLA, the rigid molecules regain their mobility and release stored energy, enabling the sample to return to its original shape, as previously described. Consequently, the shape memory rate increases with the proportion of PLA in the TPU/PLA blend. This occurs because the net-point in the blends is in the PLA crystalline phase and the switching phase in the blends is the PLA amorphous region. This phenomenon was also discovered by Wang et al. [43] and Boyacioglu et al. [18]. When the setting temperature increased to 70–80°C, and the recovery temperature to 75–85°C, the shape recovery time gradually decreased. However, the recovery time at 85°C when set to 80°C takes longer than the recovery time at 85°C when set to 70°C. And when set to 90°C, shape recovery is only possible up to 75%, and complete recovery is impossible. As shown in the DSC analysis results, PLA T_g acts as the T_{trans} of the sample, and the shape memory performance occurs in the range of 60–75°C. As the recovery temperature increases, the shape recovery slows down and the TPU chains lose their net-point

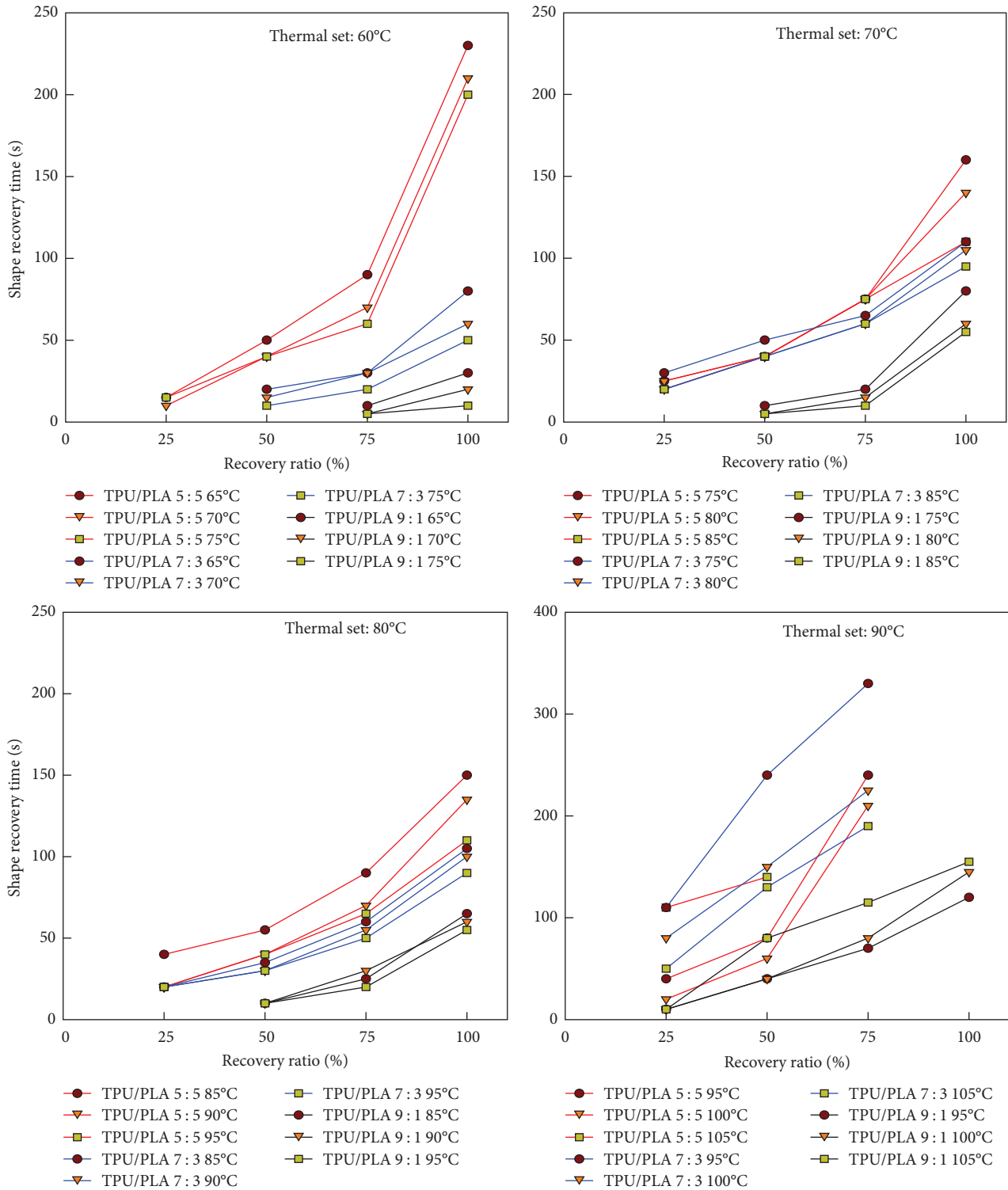


FIGURE 8: Curves of shape recovery time and recovery ratio of 3D-printed TPU/PLA blend samples with temperature stimulus.

to hold shape due to the T_g (95°C) of the HS serving as physical crosslinking. Therefore, in the case of the TPU/PLA 5:5 sample, setting at 70°C and recovering at 85°C are the most suitable conditions for shape recovery.

3.4.2. For TPU/PLA 7:3. As the TPU content increases, shape setting is impossible at 60°C due to the PLA T_{trans}

peak drop, but it is possible in the range of 70–90°C. Although it is possible to set the shape at 90°C, it is impossible to fully restore it to its original state. With the increases of the TPU content, the melting of the soft TPU segment at 85–95°C contributes to the shape recovery, showing the fastest recovery speed when set at 80°C and shape recovery at 95°C. However, if the setting temperature is 90°C, the setting

works fine, but the shape recovery ability drops above 95°C, which prevents complete recovery. This is because the amount of net shape supporting points shape is relatively reduced due to the T_g of the hard TPU segment, which is relatively greater than the support effect of PLA where crystallization occurred in this temperature range. Therefore, in the case of the TPU/PLA 7:3 sample, setting it at 80°C and recovering at 95°C is the most suitable condition.

In the case of 9:1, which has the highest TPU content, the influence of T_{trans} on PLA T_g is minimal, making it challenging to set the shape below 80°C. Shape setting becomes feasible at 90°C, and the shape recovery process is expedited when the temperature reaches 95°C.

Generally, shape recovery is achievable within the T_g of PLA (60°C) and the T_m of the TPU SS (80°C), and this phenomenon is contingent on the ratio of PLA and TPU content. As the TPU content increases, it becomes possible to set the shape at a relatively elevated temperature, while the shape recovery time tends to accelerate. It is imperative to note that for highly efficient shape fixing, it is essential for the molecular switches to permeate throughout the entire material. A favorable shape memory effect is contingent on achieving both a substantial shape-fixing ratio and an efficient shape recovery ratio.

4. Conclusions

TPU/PLA filaments for FDM 3D printers for 4D soft actuator applications have been successfully fabricated using commercial TPU 75 Shore A and PLA. The filament extrusion temperature of the TPU/PLA blends was set in the range of 189–192°C, which was higher with the increase in the PLA share. The Shore A hardness also increased with the PLA ratio from 86 to 94 A. Regarding the morphology properties of the TPU/PLA filaments, the good miscibility state was confirmed by cross- and side-sectional photos. Nevertheless, it is worth noting that no chemical reactions occurred during the melt blending process, as evidenced by the absence of any new chemical bonds identified in the FTIR results. The results of the thermal properties of the TPU/PLA filaments showed that the transition temperature of SS T_m , which is the temperature for shape memory performance, appeared at about 60–80°C by blending with PLA. The DMA results of the TPU/PLA filaments also showed that T_g peaks appeared for each polymer, and the only difference in peak intensity was due to the mechanical miscibility that occurred. A delay in degradation was observed for the TPU/PLA blends from the TGA onset temperature, which can be attributed to the increased TPU ratio. In order to determine the crystalline miscibility information between TPU and PLA, an XRD measurement was performed. In the filament state, the peak caused by the TPU HS appeared as a wide single peak at $2\theta = 20^\circ$ due to the addition of PLA and the high cooling rate of the extrusion process. However, in the heat-treated film, a unique PLA crystallization peak appeared even when blended with TPU, indicating that TPU and PLA did not mix.

The mechanical property results for the TPU/PLA filaments revealed a wide range of initial modulus values,

increasing from 5.9 ± 0.09 to 1207.6 ± 0.35 MPa, with the increase being attributed to PLA's stiffness. The tensile strength and elongation at break exhibited a considerable variation, ranging from strong and brittle to strong and ductile, with stress values spanning from 20.99 to 25.21 MPa and strain values ranging from 12.49% to 600.98%. The TPU/PLA 5:5 sample was very stiff and strong, but as the TPU content increased, its properties changed to tough and soft. The optimal temperature of the TPU/PLA filament for the 3D printer was 210°C for TPU/PLA 5:5 and 220°C for TPU/PLA 7:3 and 9:1. In the shape memory test, shape recovery is attainable within the temperature range encompassing the T_g of PLA (60°C) and the T_m (80°C) of the TPU SS, and this capability is influenced by the ratio of PLA and TPU content. The higher the TPU content, the higher the shape setting, but the faster the shape recovery time. For the TPU/PLA 5:5 sample, setting at 70°C and recovering at 85°C is the most suitable condition for shape recovery, and for the TPU/PLA 7:3 sample, setting at 80°C and recovering at 95°C is the most suitable condition. In the case of TPU/PLA 9:1, shape setting is possible at 90°C and shape recovery at 95°C takes the least amount of time. In conclusion, it is possible to manufacture filaments for 3D printers using TPU/PLA blend, and the development of 4D structures becomes possible as the shape memory performance of TPU/PLA blend by temperature stimulation appears.

Data Availability

The figures and tables data used to support the findings of this study are included within the article.

Conflicts of Interest

The authors have no conflicts of interest to disclose.

Acknowledgments

This research was supported by a grant (2021R1A4A1022059) of the Basic Science Research Program of the National Research Foundation (NRF) funded by the Ministry of Education, Republic of Korea.

References

- [1] R. Tao, L. Xi, W. Wu et al., "4D printed multi-stable metamaterials with mechanically tunable performance," *Composite Structures*, vol. 252, Article ID 112663, 2020.
- [2] S. Miao, H. Cui, M. Nowicki et al., "Stereolithographic 4D bioprinting of multiresponsive architectures for neural engineering," *Advanced Biosystems*, vol. 2, no. 9, Article ID 1800101, 2018.
- [3] Q. Zhang, X. Kuang, S. Weng et al., "Rapid volatilization induced mechanically robust shape-morphing structures toward 4D printing," *ACS Applied Materials & Interfaces*, vol. 12, no. 15, pp. 17979–17987, 2020.
- [4] A. S. Gladman, E. A. Matsumoto, R. G. Nuzzo, L. Mahadevan, and J. A. Lewis, "Biomimetic 4D printing," *Nature Materials*, vol. 15, no. 4, pp. 413–418, 2016.
- [5] W. Wang, C. Y. Yu, P. A. A. Serrano, and S. Ahn, "Soft grasping mechanisms composed of shape memory polymer

- based self-bending units,” *Composites Part B: Engineering*, vol. 164, pp. 198–204, 2019.
- [6] B. An, Y. Tao, J. Gu et al., “Thermorph: democratizing 4D printing of self-folding materials and interfaces,” in *Proceedings of the 2018 CHI Conference on Human Factors in Computing Systems*, pp. 1–12, Montreal, Canada, 2018.
- [7] Y. Wang and X. Li, “4D-printed bi-material composite laminate for manufacturing reversible shape-change structures,” *Composites Part B: Engineering*, vol. 219, Article ID 108918, 2021.
- [8] U. Kalsoom, P. N. Nesterenko, and B. Paull, “Recent developments in 3D printable composite materials,” *RSC Advances*, vol. 6, no. 65, pp. 60355–60371, 2016.
- [9] R. D. Farahani, M. Dubé, and D. Therriault, “Three-dimensional printing of multifunctional nanocomposites: manufacturing techniques and applications,” *Advanced Materials*, vol. 28, no. 28, pp. 5794–5821, 2016.
- [10] H. Li, Y. Gao, S. Zhao et al., “Dual and triple shape memory properties of poly(ϵ -caprolactone)-based cross-linked polymer elastomers,” *Polymer Testing*, vol. 115, Article ID 107738, 2022.
- [11] G. Li and W. Xu, “Thermomechanical behavior of thermoset shape memory polymer programmed by cold-compression: testing and constitutive modeling,” *Journal of the Mechanics and Physics of Solids*, vol. 59, no. 6, pp. 1231–1250, 2011.
- [12] N. Toshikj, J.-J. Robin, M. Ramonda, S. Catrouillet, and S. Blanquer, “Photo-cross-linked poly(trimethylene carbonate)/poly(ϵ -caprolactone) triblock copolymers with controlled architectures: from phase-separated structures to shape-memory materials,” *ACS Applied Polymer Materials*, vol. 3, no. 10, pp. 4966–4976, 2021.
- [13] J. Hu, Z. Feng, X. Xu et al., “UV reconfigurable shape memory polyurethane with a high recovery ratio under large deformation,” *Industrial & Engineering Chemistry Research*, vol. 60, no. 5, pp. 2144–2153, 2021.
- [14] M. Shibata, Y. Inoue, and M. Miyoshi, “Mechanical properties, morphology, and crystallization behavior of blends of poly(L-lactide) with poly(butylene succinate-co-L-lactate) and poly(butylene succinate),” *Polymer*, vol. 47, no. 10, pp. 3557–3564, 2006.
- [15] H. Hong, J. Wei, Y. Yuan et al., “A novel composite coupled hardness with flexibility—polylactic acid toughen with thermoplastic polyurethane,” *Journal of Applied Polymer Science*, vol. 121, no. 2, pp. 855–861, 2011.
- [16] S.-M. Lai and Y.-C. Lan, “Shape memory properties of melt-blended polylactic acid (PLA)/thermoplastic polyurethane (TPU) bio-based blends,” *Journal of Polymer Research*, vol. 20, Article ID 140, 2013.
- [17] J. Leng, J. Wu, and J. Zhang, “Preparation of thermoplastic polyurethane parts reinforced with in situ polylactic acid microfibrils during fused deposition modeling: the influences of deposition-induced effects,” *Industrial & Engineering Chemistry Research*, vol. 58, no. 47, pp. 21476–21484, 2019.
- [18] S. Boyacioglu, M. Kodal, and G. Ozkoc, “A comprehensive study on shape memory behavior of PEG plasticized PLA/TPU bio-blends,” *European Polymer Journal*, vol. 122, Article ID 109372, 2020.
- [19] Y. Tao, J. Shao, P. Li, and S. Q. Shi, “Application of a thermoplastic polyurethane/polylactic acid composite filament for 3D-printed personalized orthosis,” *Materials and Technologies*, vol. 53, no. 1, pp. 71–76, 2019.
- [20] X. Jing, H.-Yang Mi, X.-Fang Peng, and L.-Sheng Turng, “The morphology, properties, and shape memory behavior of polylactic acid/thermoplastic polyurethane blends,” *Polymer Engineering and Science*, vol. 55, no. 1, pp. 70–80, 2015.
- [21] E. J. Shin, Y. Park, Y. S. Jung, H. Y. Choi, and S. Lee, “Fabrication and characteristics of flexible thermoplastic polyurethane filament for fused deposition modeling three-dimensional printing,” *Polymer Engineering and Science*, vol. 62, no. 9, pp. 2947–2957, 2022.
- [22] E. J. Shin, Y. S. Jung, H. Y. Choi, and S. Lee, “Synthesis and fabrication of bio-based thermoplastic polyurethane filament for FDM 3D printing,” *Journal of Applied Polymer Science*, vol. 139, no. 40, Article ID e52959, 2022.
- [23] M. Charlon, B. Heinrich, Y. Matter, E. Couzigné, B. Donnio, and L. Avérous, “Synthesis, structure, and properties of fully bio-based thermoplastic polyurethanes, obtained from a diisocyanate based on modified dimer fatty acids, and different renewable diols,” *European Polymer Journal*, vol. 61, pp. 197–205, 2014.
- [24] A. A. A. Hakim, M. Nassar, A. Emam, and M. Sultan, “Preparation and characterization of rigid polyurethane foam prepared from sugar-cane bagasse polyol,” *Materials Chemistry and Physics*, vol. 129, no. 1–2, pp. 301–307, 2011.
- [25] A. Zlatanić, C. Lava, W. Zhang, and Z. S. Petrović, “Effect of structure on properties of polyols and polyurethanes based on different vegetable oils,” *Journal of Polymer Science Part B: Polymer Physics*, vol. 42, no. 5, pp. 809–819, 2004.
- [26] P. Alagi and S. C. Hong, “Vegetable oil-based polyols for sustainable polyurethanes,” *Macromolecular Research*, vol. 23, no. 12, pp. 1079–1086, 2015.
- [27] T. Gurunathan, S. Mohanty, and S. K. Nayak, “Isocyanate terminated castor oil-based polyurethane prepolymer: synthesis and characterization,” *Progress in Organic Coatings*, vol. 80, pp. 39–48, 2015.
- [28] J. Datta and E. Głowińska, “Effect of hydroxylated soybean oil and bio-based propanediol on the structure and thermal properties of synthesized bio-polyurethanes,” *Industrial Crops and Products*, vol. 61, pp. 84–91, 2014.
- [29] Z. Dong, Y. Li, and Q. Zou, “Degradation and biocompatibility of porous nano-hydroxyapatite/polyurethane composite scaffold for bone tissue engineering,” *Applied Surface Science*, vol. 255, no. 12, pp. 6087–6091, 2009.
- [30] X.-Z. Yang, Y.-C. Wang, L.-Y. Tang, H. Xia, and J. Wang, “Synthesis and characterization of amphiphilic block copolymer of polyphosphoester and poly(L-lactic acid),” *Journal of Polymer Science Part A: Polymer Chemistry*, vol. 46, no. 19, pp. 6425–6434, 2008.
- [31] A. Saralegi, L. Rueda, B. Fernández-D’Arlas, I. Mondragon, A. Eceiza, and M. A. Corcuera, “Thermoplastic polyurethanes from renewable resources: effect of soft segment chemical structure and molecular weight on morphology and final properties,” *Polymer International*, vol. 62, no. 1, pp. 106–115, 2013.
- [32] A. Eceiza, M. D. Martin, K. de la Caba et al., “Thermoplastic polyurethane elastomers based on polycarbonate diols with different soft segment molecular weight and chemical structure: mechanical and thermal properties,” *Polymer Engineering and Science*, vol. 48, no. 2, pp. 297–306, 2008.
- [33] M. Spirkova, J. Pavlicevic, A. Strachota et al., “Novel polycarbonate-based polyurethane elastomers: composition-property relationship,” *European Polymer Journal*, vol. 47, no. 5, pp. 959–972, 2011.
- [34] M. Asensio, V. Costa, A. Nohales, O. Bianchi, and C. M. Gómez, “Tunable structure and properties of segmented thermoplastic polyurethanes as a function of flexible segment,” *Polymer*, vol. 11, no. 12, Article ID 1910, 2019.

- [35] H.-Y. Mi, M. R. Salick, X. Jing et al., "Characterization of thermoplastic polyurethane/poly(lactic acid) (TPU/PLA) tissue engineering scaffolds fabricated by microcellular injection molding," *Materials Science and Engineering: C*, vol. 33, no. 8, pp. 4767–4776, 2013.
- [36] C. C. Hornat and M. W. Urban, "Shape memory effects in self-healing polymers," *Progress in Polymer Science*, vol. 102, Article ID 101208, 2020.
- [37] R. J. Spontak and N. P. Patel, "Thermoplastic elastomers: fundamentals and applications," *Current Opinion in Colloid & Interface Science*, vol. 5, no. 5-6, pp. 333–340, 2000.
- [38] W. Lei, C. Fang, X. Zhou, Y. Cheng, R. Yang, and D. Liu, "Morphology and thermal properties of polyurethane elastomer based on representative structural chain extenders," *Thermochimica Acta*, vol. 653, pp. 116–125, 2017.
- [39] M. Kirpluks, U. Cabulis, A. Ivdre, M. Kuranska, M. Zieleniewska, and M. Auguscik, "Mechanical and thermal properties of high-density rigid polyurethane foams from renewable resources," *Journal of Renewable Materials*, vol. 4, no. 1, pp. 86–100, 2016.
- [40] V. Pistor, D. de Conto, F. G. Ornaghi, and A. J. Zattera, "Microstructure and crystallization kinetics of polyurethane thermoplastics containing trisilanol isobutyl POSS," *Journal of Nanomaterials*, vol. 2012, Article ID 283031, 8 pages, 2012.
- [41] M. Fuensanta and J. M. Martín-Martínez, "Structural and viscoelastic properties of thermoplastic polyurethanes containing mixed soft segments with potential application as pressure sensitive adhesives," *Polymers*, vol. 13, no. 18, Article ID 3097, 2021.
- [42] E. M. Inácio, D. H. S. Souza, and M. L. Dias, "Thermal and crystallization behavior of PLA/PLLA-grafting cellulose nanocrystal," *Materials Sciences and Applications*, vol. 11, no. 1, pp. 44–57, 2020.
- [43] W. Wang, P. Ping, X. Chen, and X. Jing, "Shape memory effect of poly(L-lactide)- based polyurethanes with different hard segments," *Polymer International*, vol. 56, no. 7, pp. 840–846, 2007.